UC Santa Barbara
UC Santa Barbara Previously Published Works

Title
Single-stranded nucleic acid elasticity arises from internal electrostatic tension

Authors
Jacobson, David R
McIntosh, Dustin B
Stevens, Mark J
et al.

Single-stranded nucleic acid elasticity arises from internal electrostatic tension

David R. Jacobson[a], Dustin B. McIntosh[a], Mark J. Stevens[b], Michael Rubinstein[c], and Omar A. Saleh[d,1]

[a]Department of Physics, University of California, Santa Barbara, CA 93106; [b]Center for Integrated Nanotechnologies, Sandia National Laboratories, Albuquerque, NM 87185; [c]Department of Chemistry, University of North Carolina, Chapel Hill, NC 27599; and [d]Materials Department and Biomolecular Science and Engineering Program, University of California, Santa Barbara, CA 93016

Understanding of the conformational ensemble of flexible polyelectrolytes, such as single-stranded nucleic acids (ssNAs), is complicated by the interplay of chain backbone entropy and salt-dependent electrostatic repulsions. Molecular elasticity measurements are sensitive probes of the statistical conformation of polymers and have elucidated ssNA conformation at low force, where electrostatic repulsion leads to a strong excluded volume effect, and at high force, where details of the backbone structure become important. Here, we report measurements of ssDNA and ssRNA elasticity in the intermediate-force regime, corresponding to 5- to 100-pN forces and 50–85% extension. These data are explained by a modified wormlike chain model incorporating an internal electrostatic tension. Fits to the elastic data show that the internal tension decreases with salt, from >5 pN under 5 mM ionic strength to near zero at 1 M. This decrease is quantitatively described by an analytical model of electrostatic screening that ascribes to the polymer an effective charge density that is independent of force and salt. Our results thus connect microscopic chain physics to elasticity and structure at intermediate scales and provide a framework for understanding flexible polyelectrolyte elasticity across a broad range of relative extensions.

single-stranded nucleic acids | flexible polyelectrolytes | force spectroscopy | electrostatics

Single-stranded nucleic acids (ssNAs) occur in many biological processes, such as RNA folding (1, 2) and DNA replication (3–5), generally in disordered conformations that fluctuate between various structures. These fluctuations create a significant entropic elasticity; thus, direct measurements of molecular elasticity (extension, X, as a function of applied force, f_{app}) constitute a powerful tool for studying the ssNA structural ensemble (6). In particular, measurements at a particular f_{app} are sensitive to the conformation within the corresponding tensile length, $k_B T / f_{app}$ (to within a scaling factor), where $k_B T$ is the thermal energy (7).

ssNA structure—and that of flexible polyelectrolytes more generally—is complicated by the strong negative charge of the molecule. Multiple electrostatic and structural length scales share a similar magnitude (roughly 1 nm), disallowing models that consider only electrostatics or only backbone structure. In an uncharged flexible chain, the key structural scale is the persistence length, l_p, defining the distance beyond which thermal fluctuations strongly bend the polymer. Electrostatic interactions introduce several competing length scales: the distance, b, between charged phosphates along the ssNA backbone; the distance over which electrostatic fields are screened in salty solution (the Debye length, κ^{-1}); and the distance at which interactions between elementary charges in water have energy $k_B T$ (the Bjerrum length, l_B).

Prior studies have elucidated ssNA elastic behavior in the low- and high-force limits. At low forces, corresponding to tensile lengths larger than κ^{-1} (i.e., $f_{app} \lesssim k_B T / \kappa^{-1}$), ssNAs exhibit an elastic response with self-avoiding (Pincus) scaling, $X \sim f^{2/3}$ (7–10). Pincus elasticity is also shown by neutral polymers; for ssNAs it depends on electrostatically determined excluded volume parameters. At high force, corresponding to tensile lengths smaller than the chemical bond length, electrostatic effects become negligible and again similar behavior is seen as in uncharged polymers (11–16).

There are no similar results, grounded in the microscopic physics of the system and verified by experiments, for the intermediate-force regime in which the local chain behavior transitions from being dominated by electrostatics to backbone structure. Because of this transition, it is only at intermediate forces that charged-chain elasticity will always deviate from neutral-chain elasticity; thus, quantification of the intermediate regime is of particular importance to understanding polyelectrolyte behavior. Intermediate elasticity has been previously explained with models incorporating an electrostatics-dependent persistence length (17–19). Some experimental agreement has been seen with these models (20, 21), but only for studies at a single salt concentration and only when invoking a strongly salt-dependent charge density (22).

In this article, we use magnetic tweezers single-molecule force spectroscopy (23) to comprehensively measure the elasticity of ssDNA and ssRNA over the domains of 5–100 pN applied force (corresponding to 50–85% relative extension) and 1–1,000 mM ionic strength. We then introduce a model that uses an internal electrostatic tension to capture the observed behavior. Finally, we combine this result with the existing knowledge at lower and higher forces to furnish a comprehensive picture of ssNA elasticity—and therefore statistical conformation—over all accessible forces.

Significance

Charged, flexible polymers, such as single-stranded nucleic acids (ssNAs), are ubiquitous in biology and technology. Quantitative description of their solution conformation has remained elusive due to the competing effects of polymer configurational freedom and salt-screened electrostatic repulsion between monomers. We investigate this by measuring the elastic response of single ssNA molecules over a range of salt concentrations. The data are well described by a model, inspired by a mean-field approach, in which intrapolymer electrostatic repulsion creates a salt-dependent internal tension whose interplay with the external force determines the elasticity. The internal tension can be related to the polymer's charge spacing; thus, our results show how mesoscopic polymer conformation emerges from microscopic structure.

Results

Elasticity Measurements. The elasticity of 1–6 μm intrinsically single-stranded NAs was measured using magnetic tweezers (23, 24), in which the molecule is attached, at one end, to the substrate and, at the other end, to a paramagnetic bead. A magnetic-field gradient exerts a force on the bead, and the resulting molecular extension is measured.

The chemical means used to synthesize the ssNAs (*Materials and Methods*) yield polydisperse samples, meaning that the chain contour length, L_c, varies from chain to chain. This typically requires leaving L_c as a free parameter in subsequent fitting; the added fitting parameter weakens the statistical significance of the results. Here, we avoid this problem by collecting data on the same molecule across a broad range of ionic strength, I; thus, the L_c parameter can be constrained and fitted globally across all of the curves.

Force-Extension Model. We model the ionic strength-dependent force-extension data by representing the pairwise repulsive interactions between charged monomers along the thermally fluctuating chain as a single internal electrostatic tension, f_{el} (Fig. 1*A*), an approach inspired by the Weiss molecular field theory of ferromagnetism (25). This internal f_{el} corresponds to an electrostatic blob size $k_B T / f_{el}$ (26). For forces higher than the upper boundary of the excluded volume regime ($f_{app} \gtrsim k_B T / \kappa^{-1}$) (27), the electrostatic blobs become aligned and f_{el} acts along the length of the chain. At yet higher forces ($f_{app} \gtrsim f_{el}$), the tensile length of the applied force becomes smaller than the electrostatic blob size and electrostatic effects become less significant. We model the elastic behavior in the electrostatics-dominated intermediate-force regime by making the substitution $f \rightarrow f_{app} + f_{el}$ in the high-force (i.e., $X > L_c/2$) expression for wormlike chain (WLC) elasticity (28) to obtain

$$X = L_c \left(1 - \sqrt{\frac{k_B T}{4 l_p (f_{app} + f_{el})}} \right), \quad \text{[1]}$$

where l_p is the bare (i.e., nonelectrostatic) persistence length. In other words, we subsume all electrostatics into f_{el} and assume that l_p represents only nonelectrostatic sources of stiffness, effectively balancing electrostatic and applied tension against neutral-chain entropic elasticity. This assumption is checked below.

An example of the effect of adding $f_{el} = 5$ pN to WLC elasticity is shown in Fig. 1*B*, in which the force-extension curve shifts to higher extension and a domain of $X \sim \log(f)$ scaling is observed. Note that this plot is limited to $X > L_c/2$, the high-force domain of the WLC elasticity. Notwithstanding this limit, we expect the behavior modeled by Eq. **1** to extend from, at low force, the crossover to the excluded volume regime ($f_{app} \sim k_B T / \kappa^{-1}$) (27) to, at high force, the transition from WLC to freely jointed chain (FJC) behavior ($f_{app} \sim k_B T l_p / a^2$, where a is the chemical bond length) (14).

Internal electrostatic tension has been invoked in prior studies to explain aspects of charged polymer behavior. This includes theoretical work on polyelectrolyte brush behavior (27), as well as work on electrostatic modulation of DNA structural transitions: the double-stranded DNA overstretching transition (29) and the base unstacking transition of poly(dA) ssDNA (30). Here, we extend the approach by carefully analyzing the balance of electrostatic tension against entropic elasticity, a universal feature of polymer behavior. A further advantage of the present approach is that it permits direct, high-resolution experimental quantification of the salt-dependent tension.

We use a continuous-WLC model to treat a system that is, physically, composed of discrete chemical bond units. The parameter l_p is thus an effective persistence length. The formal
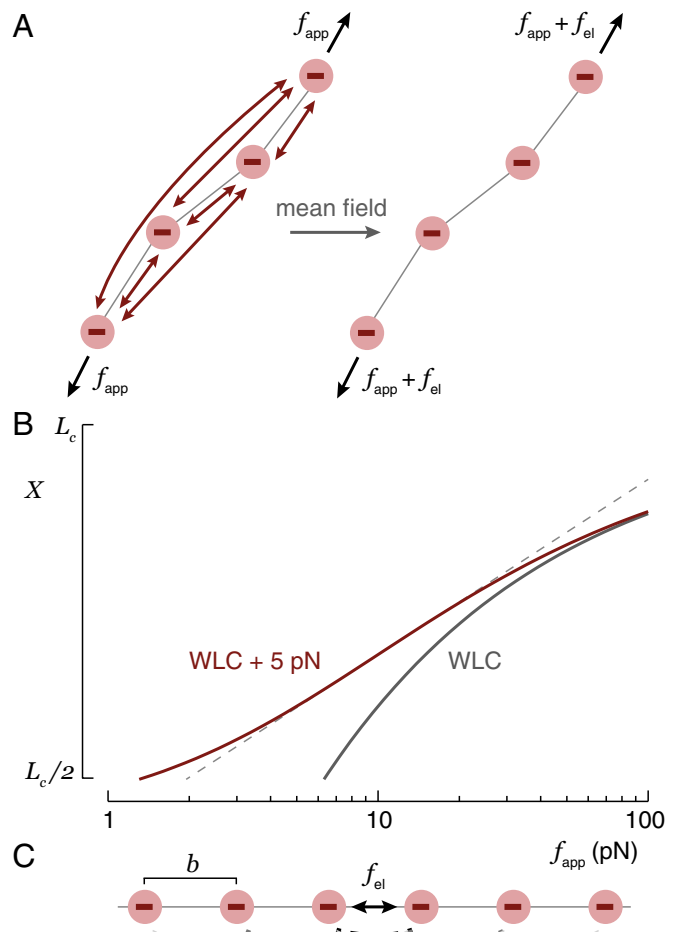

Fig. 1. (*A*) If a polyelectrolyte is stretched, the applied force, f_{app}, acts uniformly along the contour of the chain. In an approximation inspired by mean-field theories, the Coulomb repulsion between charges can be similarly treated as a uniform tension, f_{el}. (*B*) Introduction of 5 pN electrostatic tension to Eq. **1** shifts the high-force WLC curve ($l_p = 0.6$ nm) to larger extension. A domain of $X \sim \log(f)$ scaling (dashed line) emerges. (*C*) The electrostatic tension can be explicitly estimated by summing all screened Coulomb forces across a particular bond in the straight-chain configuration.

definition of l_p requires an exponential decay in the correlation between chain tangent vectors with separation; in contrast, simulations indicate that charged, flexible chains exhibit a power-law decay of tangent vector correlations for small separations (31). Nonetheless, the WLC model has been shown empirically to describe high-salt (i.e., fully screened) ssNA elasticity data (9, 10).

The high-force transition from WLC to FJC behavior occurs due to the discrete nature of backbone bonds (11–14). Based on the arguments of Dobrynin et al. (14), and on fitting the WLC–FJC interpolation function of those authors to our data, we conclude that this transition occurs at a force just above those we probed. As such, our data do not have the power to constrain the extra fitting parameter, a, that would be needed to implement that model.

Fits of Eq. **1** to representative data are shown in Fig. 2 *A* and *B*. Because data for each molecule were collected across a broad range of I, we were able to constrain L_c and l_p globally across all curves and fitted only f_{el} on a per-curve basis. In this way, N force-extension curves—each with 11–26 data points—are fitted with $N + 2$ parameters. Fits to all molecules studied are shown in *SI Appendix*, Fig. S1.
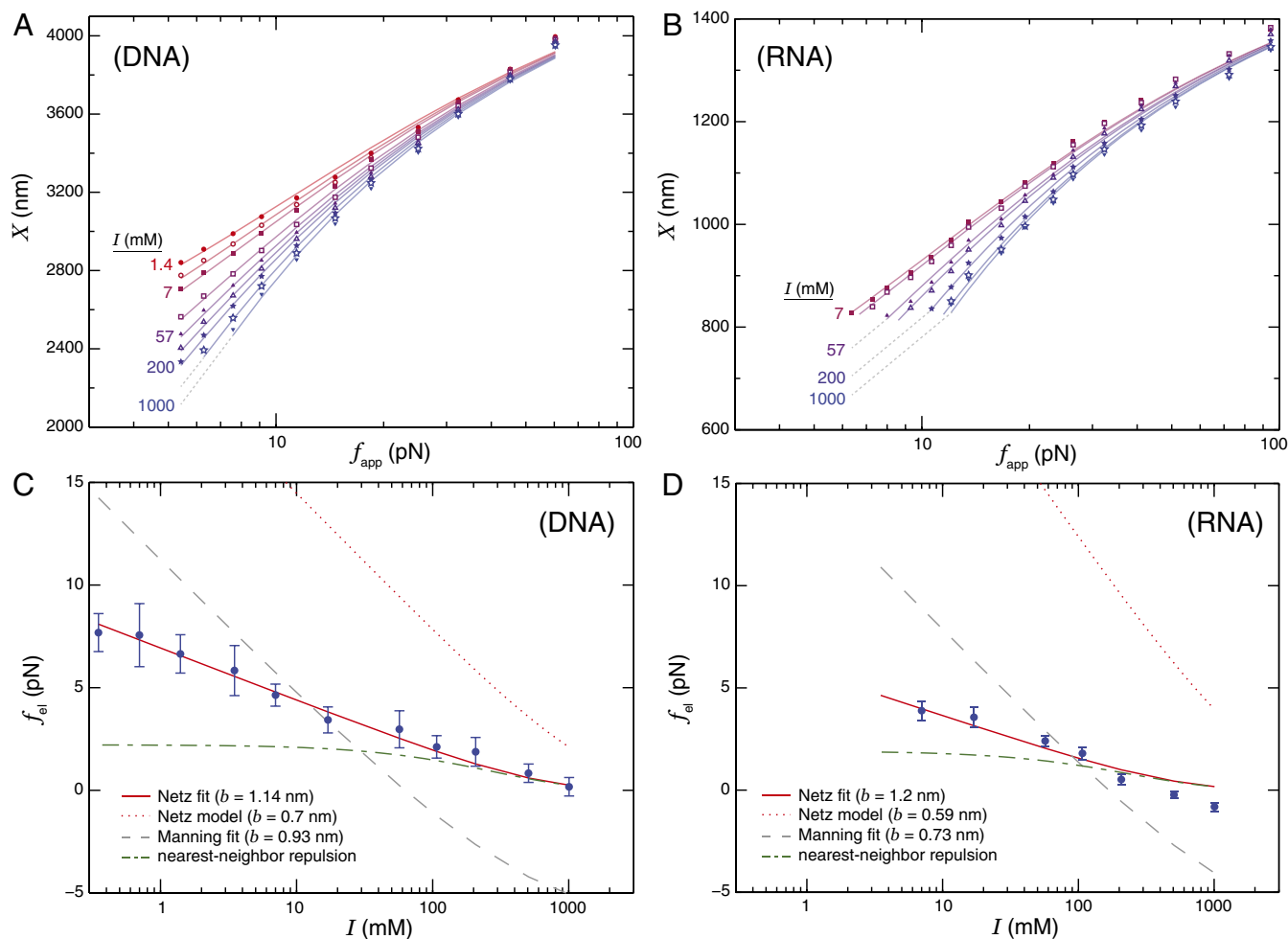
Fig. 2. (*A* and *B*) Force-extension curves of a representative (*A*) ssDNA molecule over $I = 1.4$–1,000 mM and (*B*) ssRNA molecule over $I = 7$–1,000 mM. The curves are fitted to Eq. **1**, with a different f_{el} value for each curve and L_c and l_p fitted globally across all of the curves for a particular molecule. We do not assume a model of f_{el} in the fitting. (*C* and *D*) Resulting values of f_{el}, combined across molecules, are plotted against I and are well fitted by the Netz model of electrostatic tension (Eq. **2**) with I-independent b. Error bars are standard errors of the mean. (*C*) DNA data are best fitted with effective charge spacing $b = 1.14 \pm 0.05$ nm (solid line), compared with the result for the 0.7-nm structural charge spacing (dotted line). (*D*) RNA data are best fitted by $b = 1.2 \pm 0.3$ nm, vs. 0.59 nm structural spacing. In both cases, the dashed line is the result of fitting the Manning model (32) (with best-fit charge spacing noted), whereas the dashed-dotted line is the Debye–Hückel force between a single pair of charges spaced by the b value given from Netz model fitting.

For ssDNA, there is an ∼2% disagreement between the data and the fit at the highest force value. This likely arises from both the 8.4-nN stretch modulus of ssDNA (16) (accounting for half of the discrepancy) and the WLC–FJC transition (11–14), neither of which are included in our fitting. A similar disagreement in some RNA molecules (*SI Appendix*, Fig. S1) likely also includes the effect of the sugar pucker transition discussed below.

Electrostatic Tension. The values of $f_{el}(I)$ obtained from fitting Eq. **1** to our data are shown, averaged across all molecules of a given species, in Fig. 2 *C* and *D*. As expected, f_{el} decreases as a function of I, consistent with greater charge screening at higher salt concentrations. We compared the $f_{el}(I)$ data to two analytical models of polyelectrolyte electrostatic tension. Both models consider the pairwise interactions between all charges along the chain (Fig. 1*C*), modulated by the effects of screening by salt ions. One model is that of Netz (29), which considers a straight chain of charges that interact in the Debye–Hückel (DH) limit through Yukawa potentials, $\sim e^{-\kappa r}/r$; this predicts

$$ f_{el} = \frac{k_B T l_B}{b^2} \left(\kappa b \frac{e^{-\kappa b}}{1 - e^{-\kappa b}} - \ln\left(1 - e^{-\kappa b}\right) \right). \quad [2] $$

The other model is that of Manning (32), which builds upon Eq. **2** by explicitly accounting for counterion condensation (33–35).

Both models were fitted to the data with only a single free parameter: the effective charge spacing, b. This need to use effective charge densities arises from the quantitative failure of the DH assumption underlying the models. The Netz model is able to fit both our DNA and RNA data with quantitative precision, whereas the Manning model disagrees qualitatively. Fitting to the Netz model returns effective charge spacings (ssDNA, $b = 1.14 \pm 0.05$ nm; ssRNA, $b = 1.2 \pm 0.3$ nm) notably larger than the structural charge spacings of elongated ssDNA (0.7 nm) and ssRNA (0.59 nm) (36). For comparison, Fig. 2 *C* and *D* also shows the Netz model evaluated with these structural separations, which differ between species due to sugar pucker; the disagreement with the data is apparent.

At the highest values of I, f_{el} is dominated by just the interaction of nearest-neighbor charge pairs; this can be seen by comparing the data to the repulsive force of a Yukawa interaction for a single-charge pair at a separation given by b from the best-fit Netz model (Fig. 2 *C* and *D*). However, as I decreases below 100 mM (corresponding to $\kappa^{-1} \approx b$), the nearest-neighbor charges contribute only a fraction of the tension.

Three-Parameter Global Fit. Using the Netz model of electrostatic tension (Eq. **2**) to specify f_{el} in our elastic model (Eq. **1**), we can describe a full, ionic strength-dependent elastic dataset using just three global fit parameters: L_c, l_p, and b. Such fits are of similar quality to those of Fig. 2 *A* and *B*. Sample global fits are given in *SI Appendix*, Fig. S2, as are comparable fits to models based on an electrostatics-dependent persistence length (*SI Appendix*, Figs. S3 and S4). Parameter values from global fits were combined across all three DNA and five RNA molecules studied and are listed in Table 1; L_c values were not combined, as they varied between molecules.

Discussion

Magnitude of Effective Charge Spacing. The empirical values of b obtained from our analysis (Table 1) are similar for ssDNA and ssRNA and are larger than the values expected based on the structural charge separation of the stretched chain. Anomalously large values of b were also seen in prior studies when Eq. **2** was applied to the ssDNA unstacking transition (30).

In both cases, these large b values mean that electrostatic repulsion is weaker than expected, an effect that likely arises from the failure of the DH approximation underlying Eq. **2**. The DH model assumes that macro-ion charge is equally offset by cation attraction and anion exclusion, i.e., that the local ionic strength near the NA is equal to the bulk value (37). However, it is known that, for highly charged chains such as ssNAs, I is significantly elevated close to the chain compared with the bulk due to preferential attraction of cations (38). For example, locally elevated ionic strength is seen in recent experiments (39) that show roughly 0.4 more ions per nucleotide in the ssNA ion atmosphere compared with the DH prediction, a result that decreases only very slowly with bulk I. This elevated ionic strength will more strongly screen electrostatic interactions than the DH prediction; thus, enforcing DH leads to an effective b value larger than the structural spacing, as we see in our fits.

Further complications to the interpretation of b could arise from the effective local dielectric constant, ϵ, in the vicinity of the chain and from related hydration effects. Because f_{el} arises from repulsion between backbone charges, the value of ϵ very close to the ssNA axis becomes important. The molecular dynamics simulations of Young et al. (40) indicate that ϵ interpolates between unity and bulk water values over the span of ∼1 nm in the vicinity of dsDNA; a similar interpolation likely occurs in the vicinity of the ssNAs. A lower local ϵ would have two opposing effects on the electrostatic tension. First, it would lead to increased interaction with cations and non-DH screening via counterion condensation (33–35), i.e., the augmented local ionic strength discussed above, leading to smaller-than-expected f_{el}. Second, a lower ϵ would also lead to stronger Coulomb repulsion between charges and a larger than expected f_{el}. Quantitative modeling of these effects would need to account for the detailed shape, hydration, and dielectric environment of the molecule.

Salt Independence of Effective Charge Spacing. The good quality of the fit of the Netz model to $f_{el}(I)$ implies that the effective charge density is independent of ionic strength, even though we posit that these effective values arise from the behavior of the local ionic strength in the vicinity of the chain. This is consistent with the weak salt concentration dependence of the ssNA ion atmosphere stoichiometry (39), indicating the persistence of non-DH screening over a broad domain of I. Put another way, the salt independence of b is consistent with the result that the exact predictions of counterion condensation theory break down only very gradually as nonnegligible ion concentrations are introduced (41).

Our empirical finding that b does not depend on I directly contradicts prior modeling of high-force ssNA elasticity (20, 21) based upon an electrostatics-dependent persistence length (17–19). Such models relied upon a highly salt-dependent charge density (22) inappropriately obtained from an effective-charge DH model (42–45) valid only in the far field and not suitable for treating interactions between neighboring charges. This charge density was seemingly validated through experiments (20, 21), but those studies were not conducted over a broad range of I and thus were not well suited to critically test salt-dependent effects. In *SI Appendix*, Fig. S4, we fit a WLC model incorporating an electrostatics-dependent persistence length derived from the charge density of Zhang et al. (22) (*SI Appendix*, section S1) to our broadly salt-dependent data and find very poor agreement.

Force Independence of Effective Charge Spacing. It might be expected that the effective charge spacing would increase with increasing force, as the chain is extended along the pulling axis. However, our model is able to fit the data using a force-independent b. This could be attributed to counterion condensation theory (33–35), which predicts that monovalent cations will accumulate in the vicinity of a chain with $b < l_B$ to reduce the effective charge spacing to l_B (0.7 nm in room temperature bulk water). As a highly charged chain is stretched, the bare charge spacing along the pulling axis increases, and fewer condensed counterions would be needed to maintain a constant effective charge spacing. We can test this charge-regulation picture by counting the released counterions, Γ; this counting is enabled by thermodynamic theory linking pairs of conjugate variables, here (f, X) and (Γ, I) (46–48). The analysis (*SI Appendix*, section S2) indicates that a significant number of condensed ions are indeed released, but the effect is not sufficient to hold b constant. For example, at $I = 1$ mM, we find that stretching from 0.4 pN to 100 pN releases 0.07 ions per nucleotide, less than the release of ≈0.37 ions per nucleotide expected from simple application of condensation theory.

Several other effects could work in concert with condensation to maintain a constant effective b vs. f. One is that our approach is not equally sensitive across all values of f. In particular, note in Fig. 1*B* that the addition of f_{el} (corresponding to a particular b through Eq. **2**) leads to a large elastic effect at low force, but has little effect at high force, relative to conventional WLC elasticity. Hence, it is the fit at low force that predominantly constrains b, rendering the experiment insensitive to potential high-force variation of b; thus, the observed b values are largely due to the low-force configuration. An alternative explanation is motivated by considering undulations in the chain, which increase at lower forces. Such undulations could maintain a constant effective b through the cancellation of two competing effects. First, increased undulations bring backbone charges closer together, increasing repulsive forces. Second, the undulations create lateral displacements of ions that misalign the repulsive forces from the pulling axis, leading to an actual internal tension that is less than that estimated in the calculation of Eq. **2**.

Recovery of Bare Persistence Length. The fitted l_p of ssDNA is in good agreement with a prior value (0.60 ± 0.02 nm) from

Table 1.   Fit parameters from global fitting of effective charge spacing, b, bare persistence length, l_p, and contour length, L_c, to each molecule using Eq. 1 with f_{el} given by Eq. 2

Species	b, nm	l_p, nm
ssDNA	1.16 ± 0.03	0.55 ± 0.04
ssRNA	1.12 ± 0.04	0.41 ± 0.04

Values were averaged across three DNA and five RNA molecules studied. Uncertainties are standard errors of the mean.

Jacobson et al.

measurements of single-molecule elasticity at low force (0.1–10 pN) in apparent theta conditions of the solvent, particularly a high-salt concentration where electrostatic interactions become negligible and the elastic response is that of an ideal chain (9). This agreement validates the basic premise of our model: that the salt-dependent electrostatic interactions are contained only in f_{el} and that l_p should take on its bare, salt-independent value.

The ssRNA persistence length, however, is considerably lower than the 0.83 ± 0.05-nm value previously reported in similar apparent-theta conditions (10). We investigated this effect by collecting ssRNA data over a wider force range (0.7–60 pN) at the previously identified high-salt condition ($I_\Theta = 4$ M). We find that fitting the data with the Marko–Siggia WLC interpolation formula (28) at high force (10–60 pN) gives $l_p = 0.43$ nm, similar to the result in Table 1. However, fitting at lower forces (0.7–10 pN) recovers a value of 0.85 nm, in agreement with the prior literature (10). Thus, we see that fitting Eq. 1 to our data does recover the bare persistence length, in keeping with our assumption that only f_{el} is electrostatics dependent, but that the bare persistence length itself is force dependent in a way that that of ssDNA is not. This may arise from the C3′-endo to C2′-endo sugar pucker isomerization, or another structural transition, in ssRNA (49, 50). Regardless of its origin, this effect introduces a complication into the analysis of the ssRNA data that is not present in the ssDNA and that may explain the negative values of f_{el} seen at large I in Fig. 2.

Conclusion

We have introduced a model of flexible polyelectrolyte elasticity in the intermediate-force domain that exploits the concept of internal electrostatic tension, f_{el}. The model is validated through its ability to reproduce experimental ssDNA and ssRNA force-extension data across a broad range of salt concentrations. Further, the internal tension can be quantified from a microscopic viewpoint, resulting in salt-dependent elasticity predictions that depend on just two structural parameters: l_p, which sets the contribution of configurational entropy to elasticity, and b, which determines the magnitude of f_{el}. The model is written as a simple, closed-form expression (Eq. 1) and the resulting values of f_{el} can be directly compared with the forces involved in other molecular processes.

The internal-tension model also naturally accounts for the transitions in polyelectrolyte elasticity through the interplay of f_{el} and f_{app}. The present results, particularly the elastic model given by Eq. 1, define the structure and elasticity in the intermediate regime, $k_B T/\kappa^{-1} \lesssim f_{app} \lesssim f_{el}$. This is the regime flanked, at lower applied force, by a self-avoidance regime where conformation and elasticity are dominated by electrostatically defined chain parameters, and at higher applied force, by a regime sensitive to structural details other than the presence and spacing of charges. Indeed, prior work on NA elasticity corroborates and quantifies this view: Measurements with sub-picoNewton applied forces (8, 10) revealed swollen-chain elasticity, $X \sim f^{2/3}$ (7), that was attributed to electrostatically controlled excluded-volume interactions. High-force ssNA elasticity has been explained by nonelectrostatic details of the chain; particularly, Dobrynin et al. (14) showed that ssNA's moderate-force WLC behavior will transition, around 60 pN, to FJC elasticity due to the discrete nature of bonds along the backbone, whereas Hugel et al. (16) found that this FJC elasticity will eventually be dominated by enthalpic stretching of backbone bonds for forces beyond a few hundred picoNewtons.

A multiregime polyelectrolyte elasticity model can be created by combining the present work with other polymer elasticity regimes. This is done in Fig. 3, where we plot the Dobrynin et al. WLC–FJC transition model (14), modified by adding
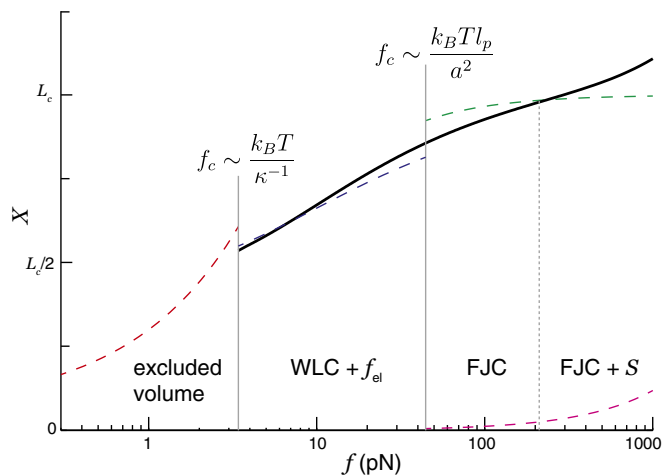

Fig. 3. The WLC model with internal electrostatic tension (WLC + f_{el}) connects the lower-force swollen-chain elastic regime, with electrostatically dominated excluded volume, to the higher-force regime dominated by the nonelectrostatic structure of the chemical backbone. Dashed lines denote the expected scaling in the different force regimes (separated by different crossover forces, f_c): $X \sim f^{2/3}$ excluded volume scaling (red), WLC with f_{el} (Eq. 1) (blue), FJC (green), and an additional contribution from the stretch modulus $S = 8.4$ nN (16) (magenta). For clarity, the expected lowest-force linear response regime is not shown. The solid line is the elastic model of Dobrynin et al. (14), modified to account for electrostatic tension and S (*SI Appendix*, section S3). A broad domain of quasi-logarithmic scaling arises from the interpolation between the excluded volume, f_{el}-modified WLC, FJC, and enthalpic stretching regimes.

an internal electrostatic tension as in Eq. 1 and by including an enthalpic stretching term (*SI Appendix*, section S3). The result is a single analytical model that describes elastic behavior over two decades of force and depends on four intensive chain parameters: persistence length, charge spacing (or, equivalently, electrostatic tension), bond length (controlling the WLC–FJC transition), and stretch modulus. Extending this line to the swollen-chain regime would add an intensive parameter (the salt-dependent excluded volume) and would require an analytical model of swollen-chain elasticity beyond the level of a scaling theory; we are unaware of such a model. The multiregime model shows a slow, near-logarithmic increase in extension over multiple decades in force, in agreement with prior experimental observations (20, 51). Thus, we find that the mean-field–inspired electrostatic tension model introduced here permits a comprehensive view of flexible polyelectrolyte elasticity.

Materials and Methods

ssNA Samples. We studied the elasticity of 1- to 6-μm ssNAs with sequences rendering them intrinsically single stranded [the eighth polypyrimidine sequence of Brockman et al. (52) for DNA and poly(U) for RNA]. DNA was synthesized, as in McIntosh et al. (30), by rolling-circle amplification (53) with a 5′ biotin-labeled primer for bead attachment; the glass substrate attachment was by nonspecific adhesion. RNA was synthesized, as in Jacobson et al. (10), by elongation of a 5′ thiol-labeled primer (for attachment to maleimide-functionalized substrate), using polynucleotide phosphorylase (54); a 3′ biotin label (bead attachment) was added using terminal deoxynucleotidyl transferase.

Elasticity Measurements. The molecular elasticity of the ssNA samples was measured using single-molecule magnetic tweezers force spectroscopy (23, 24). The molecule under study was attached, at one end, to the surface of a glass coverslip and, at the other end, to a micrometer-scale paramagnetic bead (2.8 μm Dynabeads M-280). A microfluidic flow cell, containing the sample, was placed in an optical microscope; rare-earth magnets above the stage established a magnetic field gradient, exerting a force on the bead

and, in turn, on the molecule. Molecular extension was measured by monitoring the diffraction ring pattern cast by the bead (24); f_{app} was calibrated by computing the Allan variance of the bead's horizontal fluctuations and fitting to a model function (55). Force-extension curves for each individual molecule studied were collected over a range of solution ionic strength (0.1–1,000 mM for DNA and 7–1,000 mM for RNA). For $I > 7$ mM, solutions were prepared by adding NaCl to a background of 10 mM Tris buffer at pH 7.5 (10 mM of this buffer corresponds to a 7-mM ionic strength). For $I < 7$ mM, the ionic strength was set by reducing the buffer concentration. Measurements of ssDNA were replicated in three different molecules; those of ssRNA were replicated in five molecules.

1. Doherty EA, Doudna JA (2001) Ribozyme structures and mechanisms. *Annu Rev Biophys Biomol Struct* 30:457–475.
2. Garst AD, Edwards AL, Batey RT (2011) Riboswitches: Structures and mechanisms. *Cold Spring Harb Perspect Biol* 3:a003533.
3. Bochkarev A, Pfuetzner RA, Edwards AM, Frappier L (1997) Structure of the single-stranded-DNA-binding domain of replication protein A bound to DNA. *Nature* 385:176–181.
4. Roe JH, Burgess RR, Record MT (1984) Kinetics and mechanism of the interaction of Escherichia coli RNA polymerase with the λP R promoter. *J Mol Biol* 176:495–522.
5. Kozlov AG, Lohman TM (1998) Calorimetric studies of E. coli SSB protein-single-stranded DNA interactions. Effects of monovalent salts on binding enthalpy. *J Mol Biol* 278:999–1014.
6. Camunas-Soler J, Ribezzi-Crivellari M, Ritort F (2016) Elastic properties of nucleic acids by single-molecule force spectroscopy. *Annu Rev Biophys* 45:65–84.
7. Pincus P (1976) Excluded volume effects and stretched polymer chains. *Macromolecules* 9:386–388.
8. Saleh O, McIntosh D, Pincus P, Ribeck N (2009) Nonlinear low-force elasticity of single-stranded DNA molecules. *Phys Rev Lett* 102:068301.
9. McIntosh D, Saleh O (2011) Salt species-dependent electrostatic effects on ssDNA elasticity. *Macromolecules* 44:2328–2333.
10. Jacobson DR, McIntosh DB, Saleh OA (2013) The snakelike chain character of unstructured RNA. *Biophys J* 105:2569–2576.
11. Rosa A, Hoang T, Marenduzzo D, Maritan A (2003) Elasticity of semiflexible polymers with and without self-interactions. *Macromolecules* 36:10095–10102.
12. Livadaru L, Netz R, Kreuzer H (2003) Stretching response of discrete semiflexible polymers. *Macromolecules* 36:3732–3744.
13. Toan NM, Thirumalai D (2010) Theory of biopolymer stretching at high forces. *Macromolecules* 43:4394–4400.
14. Dobrynin AV, Carrillo JMY, Rubinstein M (2010) Chains are more flexible under tension. *Macromolecules* 43:9181–9190.
15. Smith SB, Cui Y, Bustamante C (1996) Overstretching B-DNA: The elastic response of individual double-stranded and single-stranded DNA molecules. *Science* 271:795–799.
16. Hugel T, Rief M, Seitz M, Gaub HE, Netz RR (2005) Highly stretched single polymers: Atomic-force-microscope experiments versus ab-initio theory. *Phys Rev Lett* 94:048301.
17. Odijk T (1977) Polyelectrolytes near the rod limit. *J Polym Sci Pol Phys* 15:477–483.
18. Skolnick J, Fixman M (1977) Electrostatic persistence length of a wormlike polyelectrolyte. *Macromolecules* 10:944–948.
19. Barrat JL, Joanny JF (1993) Persistence length of polyelectrolyte chains. *Europhys Lett* 24:333–338.
20. Dessinges MN, et al. (2002) Stretching single stranded DNA, a model polyelectrolyte. *Phys Rev Lett* 89:248102.
21. Seol Y, Skinner GM, Visscher K (2004) Elastic properties of a single-stranded charged homopolymeric ribonucleotide. *Phys Rev Lett* 93:118102.
22. Zhang Y, Zhou H, Ou-Yang ZC (2001) Stretching single-stranded DNA: Interplay of electrostatic, base-pairing, and base-pair stacking interactions. *Biophys J* 81:1133–1143.
23. De Vlaminck I, Dekker C (2012) Recent advances in magnetic tweezers. *Annu Rev Biophys* 41:453–472.
24. Ribeck N, Saleh OA (2008) Multiplexed single-molecule measurements with magnetic tweezers. *Rev Sci Instrum* 79:094301.
25. Weiss P (1907) The hypothesis of the molecular field and the ferromagnetic property. *J Phys Theor Appl* 6:661–690.
26. de Gennes PG, Pincus P, Velasco RM, Brochard F (1976) Remarks on polyelectrolyte conformation. *J Phys Theor Appl* 37:1461–1473.
27. Zhulina EB, Rubinstein M (2012) Ionic strength dependence of polyelectrolyte brush thickness. *Soft Matter* 8:9376–9383.
28. Marko J, Siggia E (1995) Stretching DNA. *Macromolecules* 28:8759–8770.
29. Netz RR (2001) Strongly stretched semiflexible extensible polyelectrolytes and DNA. *Macromolecules* 34:7522–7529.
30. McIntosh DB, Duggan G, Gouil Q, Saleh OA (2014) Sequence-dependent elasticity and electrostatics of single-stranded DNA: Signatures of base-stacking. *Biophys J* 106:659–666.
31. Toan NM, Thirumalai D (2012) On the origin of the unusual behavior in the stretching of single-stranded DNA. *J Chem Phys* 136:235103.
32. Manning GS (2006) The persistence length of DNA is reached from the persistence length of its null isomer through an internal electrostatic stretching force. *Biophys J* 91:3607–3616.
33. Oosawa F (1957) A simple theory of thermodynamic properties of polyelectrolyte solutions. *J Polym Sci* 23:421–430.
34. Imai N, Onishi T (1959) Analytical solution of Poisson-Boltzmann equation for two-dimensional many-center problem. *J Chem Phys* 30:1115–1116.
35. Manning GS (1969) Limiting laws and counterion condensation in polyelectrolyte solutions I. Colligative properties. *J Chem Phys* 51:924–933.
36. Salamone J, ed (1996) *Polymeric Materials Encyclopedia* (CRC, Boca Raton, FL), pp 649–650.
37. Landy J, McIntosh D, Saleh O, Pincus P (2012) Ionic excesses and entropies in mean-field screening models. *Soft Matter* 8:9368–9375.
38. Jacobson DR, Saleh OA (2017) Counting the ions surrounding nucleic acids *Nucleic Acids Res* 87:1596–1605.
39. Jacobson DR, Saleh OA (2016) Quantifying the ion atmosphere of unfolded, single-stranded nucleic acids using equilibrium dialysis and single-molecule methods. *Nucleic Acids Res* 44:3763–3771.
40. Young M, Jayaram B, Beveridge D (1998) Local dielectric environment of B-DNA in solution: Results from a 14 ns molecular dynamics trajectory. *J Phys Chem B* 102:7666–7669.
41. Manning GS (1977) Limiting laws and counterion condensation in polyelectrolyte solutions: IV. The approach to the limit and the extraordinary stability of the charge fraction. *Biophys Chem* 7:95–102.
42. Neukirch S, Marko JF (2011) Analytical description of extension, torque, and super-coiling radius of a stretched twisted DNA. *Phys Rev Lett* 106:138104.
43. Ubbink J, Odijk T (1999) Electrostatic-undulatory theory of plectonemically super-coiled DNA. *Biophys J* 76:2502–2519.
44. Stroobants A, Lekkerkerker H, Odijk T (1986) Effect of electrostatic interaction on the liquid crystal phase transition in solutions of rodlike polyelectrolytes. *Macromolecules* 19:2232–2238.
45. Stigter D (1975) The charged colloidal cylinder with a Gouy double layer. *J Colloid Interf Sci* 53:296–306.
46. Zhang H, Marko JF (2008) Maxwell relations for single-DNA experiments: Monitoring protein binding and double-helix torque with force-extension measurements. *Phys Rev E* 77:031916.
47. Landy J, McIntosh D, Saleh O (2012) Quantifying screening ion excesses in single-molecule force-extension experiments. *Phys Rev Lett* 109:048301.
48. Jacobson DR, Saleh OA (2015) Measuring the differential stoichiometry and energetics of ligand binding to macromolecules by single-molecule force spectroscopy: An extended theory. *J Phys Chem B* 119:1930–1938.
49. Saenger W (1984) *Principles of Nucleic Acid Structure* (Springer, New York).
50. Foloppe N, MacKerell AD (1998) Conformational properties of the deoxyribose and ribose moieties of nucleic acids: A quantum mechanical study. *J Phys Chem B* 102:6669–6678.
51. Rief M, Clausen-Schaumann H, Gaub HE (1999) Sequence-dependent mechanics of single DNA molecules. *Nat Struct Mol Biol* 6:346–349.
52. Brockman C, Kim SJ, Schroeder CM (2011) Direct observation of single flexible polymers using single stranded DNA. *Soft Matter* 7:8005–8012.
53. Wickersham CE, Kerr DH, Lipman EA (2010) Synthesis of extended nanoscale optical encoders. *Bioconjug Chem* 21:2234–2238.
54. van den Hout M, Skinner GM, Klijnhout S, Krudde V, Dekker NH (2011) The passage of homopolymeric RNA through small solid-state nanopores. *Small* 7:2217–2224.
55. Lansdorp BM, Saleh OA (2012) Power spectrum and Allan variance methods for calibrating single-molecule video-tracking instruments. *Rev Sci Instrum* 83:025115.